Astrocyte immunometabolic regulation of the tumor microenvironment drives glioblastoma pathogenicity

Rita Perelroizen[1,†], Bar Philosof[1,†], Noga Budick-Harmelin[2], Tom Chernobylsky[2], Ariel Ron[1], Katzir Rotem[3], Dor Shimon[2], Adi Tessler[2], Orit Adir[2], Anat Gaoni-Yogev[2], Tom Meyer[1], Avivit Krivitsky[2], Nuphar Shidlovsky[2], Asaf Madi[4], Ruppin Eytan[3] and Lior Mayo[1,2*]

Supplementary material:

1. Supplementary Figures 1-8
2. Supplementary Tables 1-3

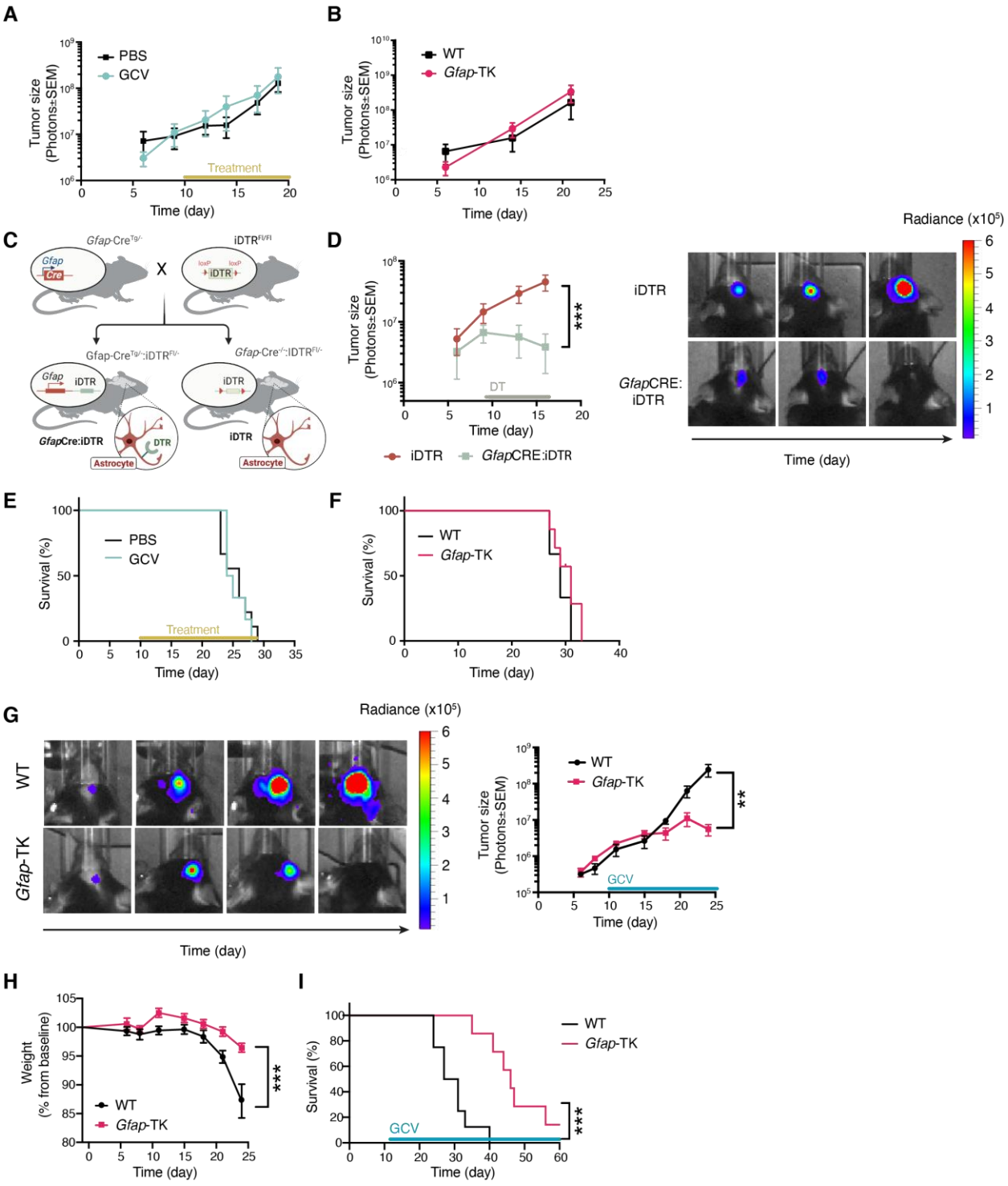

Supplementary Figure 1. Tumor-associated astrocyte depletion halts glioblastoma progression. (**A-B**) Tumor size of GL261-bearing mice as determined by bioluminescence imaging. **A**, GL261 cells were intracranially implanted into WT mice. GBM-bearing mice were treated daily with Ganciclovir (GCV, 25mg/kg) or vehicle (PBS) from day 10 until the

experimental end. Data are representative of two independent experiments with n = 8 mice/group. (**B**) GL261 cells were intracranially implanted into WT or *Gfap*-TK mice. Data are representative of two independent experiments with *n* = 7 mice/group. (**C**) *Gfap*CRE:iDTR breeding scheme. Mice in which the expression of the DT receptor (DTR) from a ubiquitously active promoter is prevented by a loxP-flanked stop cassette (iDTR)[1] were crossed with transgenic mice expressing the Cre recombinase under the control of the GFAP promoter to generate *Gfap*CRE:iDTR mice, in which DTR expression is limited to $GFAP^+$ astrocytes, resulting in their depletion following DT-A administration[2]. (**D**) iDTR or *Gfap*CRE:iDTR littermates, were intracranially implanted with GL261. Ten days later mice were treated daily with DT-A (1100ng/mice nasally). Tumor size was analyzed by bioluminescence imaging. Data are representative of two independent experiments with *n* = 7 mice/group. (**E-F**) Kaplan-Meier curves assess the overall survival of mice from **A** and **B**, respectively. (**G-I**) Astrocyte ablation halts CT-2A glioma pathogenicity. CT-2A glioma cells were intracranially implanted into WT or *Gfap*-TK littermates and treated with GCV as in (**Fig 1D**). Tumor growth was analyzed by bioluminescence imaging (**G**), and mice weight loss and survival were monitored (**H** and **I**, respectively). Data in **A,B,D,G**, and **H** are shown as mean ± s.e.m. *P* values were determined by two-way ANOVA (**A,B,D,G**, and **H**) or Log rank (Mantel-Cox) test (**E**,**F** and **I**)). $^{**}P<0.01$, $^{***}P<0.001$.

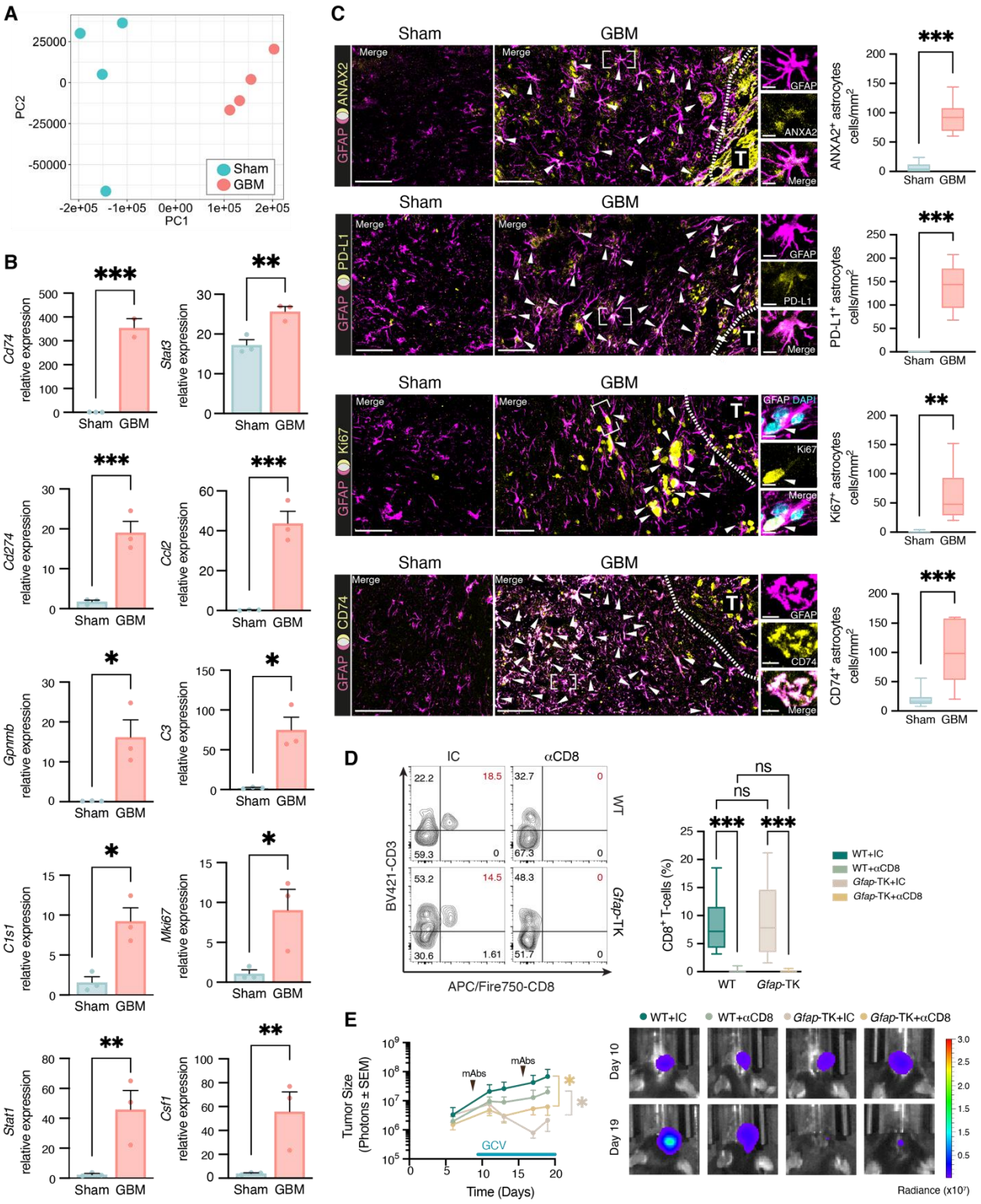

Supplementary Figure 2. Transcriptomic analysis of tumor-associated astrocytes. (A) PCA of differentially regulated genes of RiboTag-isolated astrocytes (as in Fig 2) from PBS-injected mice (Sham, pink) or GL261 GBM-bearing mice (GBM, blue). PC1 was associated with the

variance within the *sham* and *GBM* data sets, whereas PC2 was associated with the variance between each group. (**B)** Validation of RNA seq data in different biological samples. qPCR analysis of *Cd274*, *Ccl2*, *Stat1*, *Cd74*, *Stat3*, *Csf1*, *Gpnmb*, *C3*, *C1s1*, and *Mki67* expression in RiboTag-isolated astrocytes from sham-injected or GBM-implanted injected mice; expression normalized to *Ppia*. Data are representative of 3 independent experiments *(n* = 3 biologically independent samples). Data are shown as mean ± s.e.m. (C) Immunohistochemistry analysis of GFAP (magenta) co-localization with Annexin A2 (ANXA2, yellow), PD-L1 (yellow), Ki67 (yellow), or CD74 (yellow) of sham-injected or GBM-bearing mice. Representative images on the left, box-plot analysis of the antigen-positive astrocytes per cm^2 (*n* = 9), on the right. Scale bars, 500 μm (left), 5 μm (right). Co-localization (white) is identified by white arrowheads. Data are shown as median, interquartile interval, minimum, and maximum values. (**D**,**E**) $CD8^+$ T-cell depletion in WT or *Gfap*-TK mice GBM-bearing mice. GL261 cells were intracranially implanted, and the mice were treated daily with GCV from day 9 until the experimental end (as in Fig 1D), and intraperitoneally injected (black arrows) with CD8 depleting mAbs (αCD8) or isotype control (IC) (0.1 mg/mouse, as in^3). Representative data of two independent experiments (*n* = 9 mice/group). (**D**) Analysis of the $CD8^+$ T-cells frequency in the blood. Representative flow cytometry plots of $CD3^+/CD8^+$ staining are shown on the left and quantification analyses of $CD8^+$ T-cells frequency are on the right. (**E**) Tumor size of GL261-bearing mice as determined by bioluminescence imaging. *P* values were determined by two-sided Student's t-tests (**B,C**) or two-way ANOVA (**D**,**E**). **P*<0.05, ***P*<0.01, ****P*<0.001.

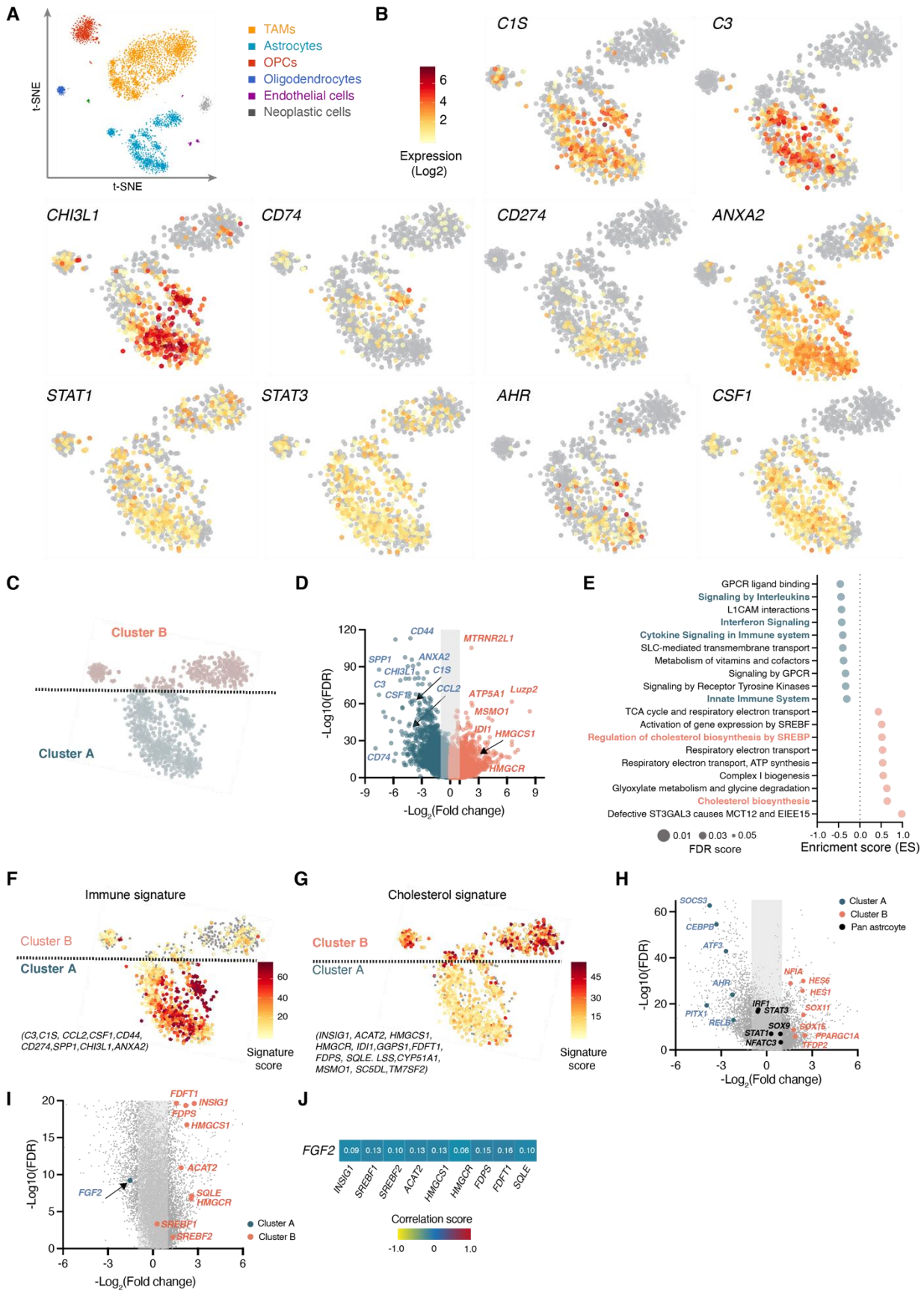
A
t-SNE
t-SNE
TAMs
Astrocytes
OPCs
Oligodendrocytes
Endothelial cells
Neoplastic cells
B
Expression (Log2)
C1S
C3
CHI3L1
CD74
CD274
ANXA2
STAT1
STAT3
AHR
CSF1
C
Cluster B
Cluster A
D
-Log10(FDR)
-Log2(Fold change)
CD44
MTRNR2L1
SPP1
ANXA2
CHI3L1
C1S
C3
CSF1
CCL2
ATP5A1
Luzp2
MSMO1
IDI1
HMGCS1
CD74
HMGCR
E
GPCR ligand binding
Signaling by Interleukins
L1CAM interactions
Interferon Signaling
Cytokine Signaling in Immune system
SLC-mediated transmembrane transport
Metabolism of vitamins and cofactors
Signaling by GPCR
Signaling by Receptor Tyrosine Kinases
Innate Immune System
TCA cycle and respiratory electron transport
Activation of gene expression by SREBF
Regulation of cholesterol biosynthesis by SREBP
Respiratory electron transport
Respiratory electron transport, ATP synthesis
Complex I biogenesis
Glyoxylate metabolism and glycine degradation
Cholesterol biosynthesis
Defective ST3GAL3 causes MCT12 and EIEE15
FDR score
Enricment score (ES)
F
Immune signature
Cluster B
Cluster A
(C3,C1S, CCL2,CSF1,CD44, CD274,SPP1,CHI3L1,ANXA2)
Signature score
G
Cholesterol signature
Cluster B
Cluster A
(INSIG1, ACAT2, HMGCS1, HMGCR, IDI1,GGPS1,FDFT1, FDPS, SQLE. LSS,CYP51A1, MSMO1, SC5DL,TM7SF2)
Signature score
H
Cluster A
Cluster B
Pan astrocyte
-Log10(FDR)
-Log2(Fold change)
SOCS3
CEBPB
ATF3
NFIA
HES6
AHR
HES1
IRF1
STAT3
SOX11
PITX1
RELB
SOX9
SOX15
STAT1
PPARGC1A
NFATC3
TFDP2
I
-Log10(FDR)
-Log2(Fold change)
FDFT1
INSIG1
FDPS
HMGCS1
ACAT2
FGF2
SQLE
HMGCR
SREBF1
SREBF2
Cluster A
Cluster B
J
FGF2
0.09 0.13 0.10 0.13 0.13 0.06 0.15 0.16 0.10
INSIG1
SREBF1
SREBF2
ACAT2
HMGCS1
HMGCR
FDPS
FDFT1
SQLE
Correlation score

Supplementary Figure 3. Transcriptomic analysis of human tumor-associated astrocytes (**A**, **B**) Analysis of single-cell data of the tumor microenvironment of IDH1^{neg} grade IV GBM patients performed on data by Darmanis et. al[4]. (**A)** unbiased clustering of the TAMs (1842 cells, orange), TAAs (1052 cells, light blue), oligodendrocyte precursor cells (OPCs, 406 cells, red), oligodendrocytes (81 cells, dark blue), and endothelial cells (50 cells, purple), neurons (21, green) and neoplastic cells (137, gray) defined based on the expression of known markers[5-7]), presented as color-coded TSNE plot. (**B)** Heat map overly of the scRANseq gene expression intensity within the astrocyte cluster of *C1S, C3, CHI3L1, CD74, CD274, ANXA2, STAT1, STAT3, AHR, and CSF1*. Expression levels are defined by color-coded expression as indicated (from yellow to red; gray coloring indicates that the transcript was not detected). (**C-H**) Analysis of astrocyte diversity. (**C,D**) Sub clustering of astrocytes based on differential expression. (**C**) Color-coded TSNE plot of cluster A (Blue, 599 cells) and cluster B (Pink, 453 cells). **(D)** Volcano plot of gene expression in astrocytes, color-coded by the cluster enrichment. (**E**) Top 20 Functional enrichment pathways (FDR<0.05) in the astrocyte clusters, color-coded by the cluster enrichment. (**F,G**) Heat map overly of the scRNAseq gene expression intensity of astrocyte immune and cholesterol signatures (**F and G, respectively**). Expression levels in heatmaps are color-coded (from yellow to red; Grey indicates that the transcript was not detected). Genes associated with each signature are stated at the bottom of the corresponding heat map. Signature score is defined as the sum of all relevant transcripts per cell. (**H**) Expression levels overlay of significant (FDR<0.001) transcription factors on volcano plot from (**D**), color-codded by association with cluster A (blue), B (pink), or expressed evenly between the two clusters (pan-astrocyte expression, black). (**I,J**) Analysis of *FGF2* expression and its correlation to cholesterol synthesis genes (*INSG1*, *SREBF1*, *SREBF2*, *ACAT2*, HMGCS1, *HMGCR*, *FDPS*, *FDFT1*, and *SQLE*), which are regulated by astrocyte cell density[8]. **(I)** Heat map overly of the transcripts expression levels in the astrocytes, color-coded by their cluster association (as in **H**). (**J**) Heat map of the Jaccard correlation index between *FGF2* transcript to the cholesterol synthesis genes. Correlation score is noted within each cell. Correlation is color-coded [negative (yellow) , natural (blue) and purple (positive)].

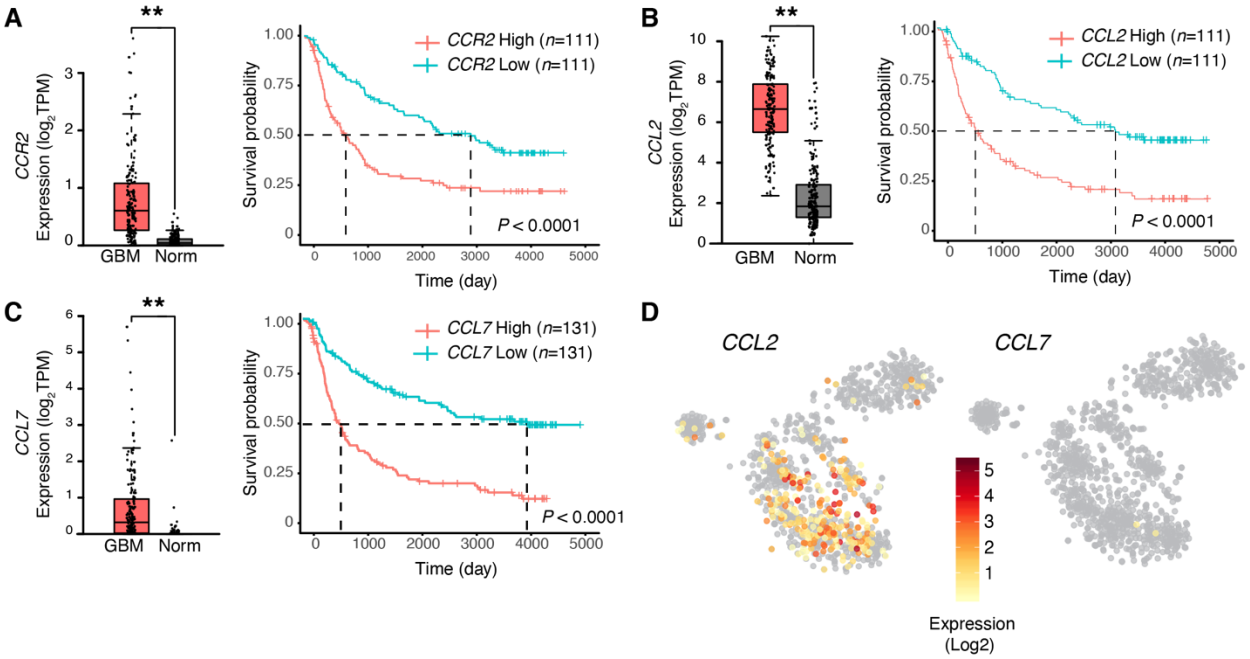

Supplementary Figure 4. Analysis of CCR2 pathway in human GBM. (A-C) Analysis of gene expression (Box plots, left panel; n=163 GBM patients and 207 normal controls) and survival correlations (Kaplan-Meier Curve, right panel; n as indicated) for *CCR2* (**A**), *CCL2* (**B**) and *CCL7* (**C**). *n* represents the number of patients per group. Data are shown as mean ± s.e.m. *P* values were determined by or two-sided Student's (expression data, **P*<0.01) or Log-rank (Mantel-Cox) tests (survival, *P*<0.0001). (**D**) Heat map overly of the scRNAseq gene expression intensity of *CCL2*, and *CCL7* in tumor-associated astrocyte cluster of GBM patients[4] (as in **Supplementary Fig 3B)**. Expression levels are defined by color-coded expression (from yellow to red; Grey indicates that the transcript was not detected).

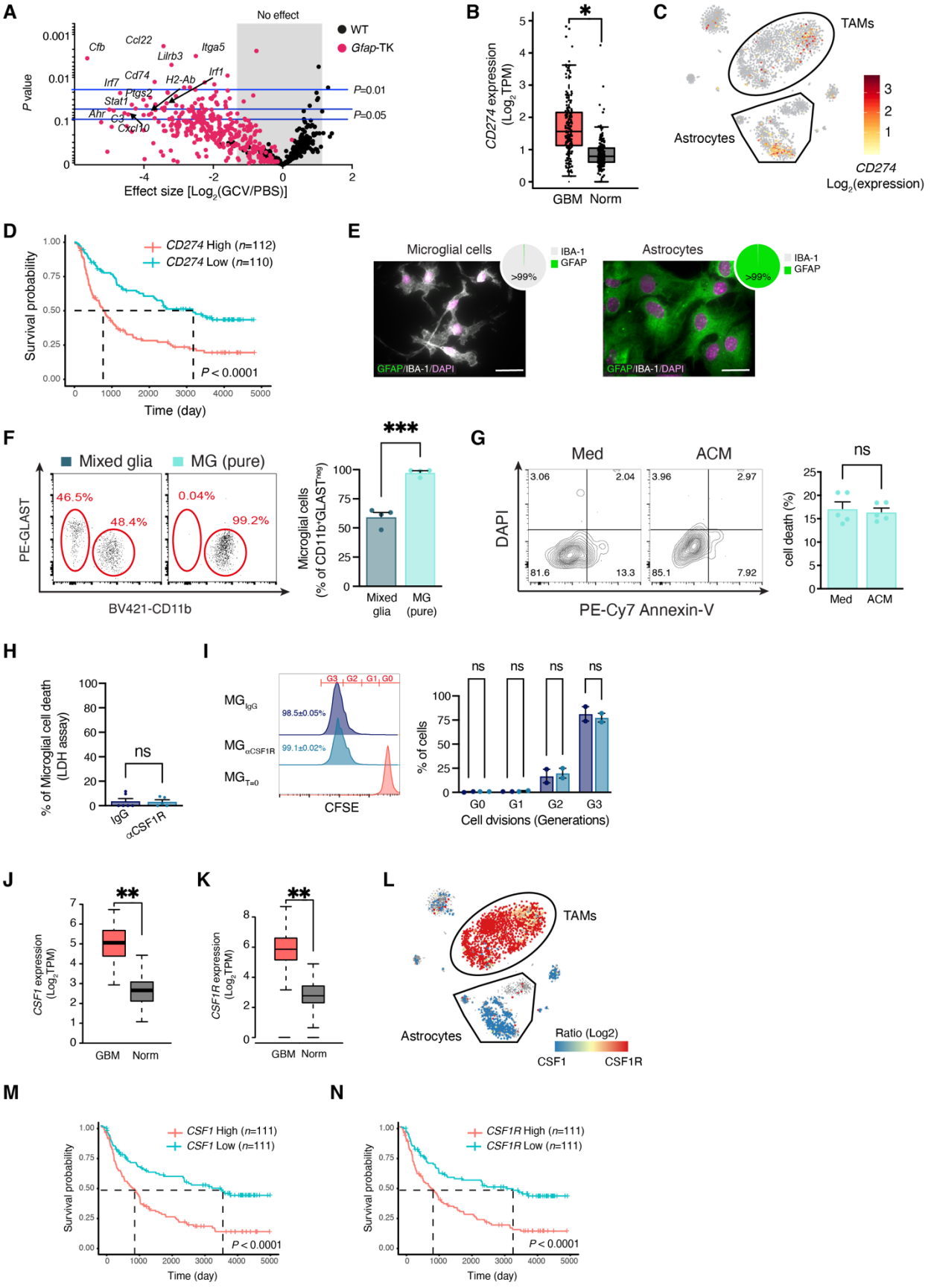
A
No effect
WT
Gfap-TK
P value
Cfb
Ccl22
Lilrb3
Itga5
Irf7
Cd74
H2-Ab
Irf1
Ptgs2
Stat1
Ahr
C3
Cxcl10
P=0.01
P=0.05
Effect size [Log2(GCV/PBS)]
B
CD274 expression (Log2TPM)
GBM Norm
C
TAMs
Astrocytes
CD274 Log2(expression)
D
CD274 High (n=112)
CD274 Low (n=110)
Survival probability
P < 0.0001
Time (day)
E
Microglial cells
Astrocytes
IBA-1
GFAP
>99%
GFAP/IBA-1/DAPI
F
Mixed glia
MG (pure)
PE-GLAST
BV421-CD11b
46.5%
48.4%
0.04%
99.2%
Microglial cells (% of CD11b+GLAST neg)
Mixed glia
MG (pure)
G
Med
ACM
DAPI
PE-Cy7 Annexin-V
3.06
2.04
81.6
13.3
3.96
2.97
85.1
7.92
cell death (%)
H
% of Microglial cell death (LDH assay)
ns
IgG
αCSF1R
I
MGIgG
MGαCSF1R
MGT=0
98.5±0.05%
99.1±0.02%
G3 G2 G1 G0
CFSE
% of cells
Cell divisions (Generations)
J
CSF1 expression (Log2TPM)
GBM Norm
K
CSF1R expression (Log2TPM)
GBM Norm
L
TAMs
Astrocytes
Ratio (Log2)
CSF1
CSF1R
M
CSF1 High (n=111)
CSF1 Low (n=111)
Survival probability
P < 0.0001
Time (day)
N
CSF1R High (n=111)
CSF1R Low (n=111)
Survival probability
P < 0.0001
Time (day)

Supplementary Figure 5. Profile of Tumor-associated Macrophages in Glioblastoma. (A) Volcano plot of differential gene expression in FACS-sorted TAMs from GCV-treated WT (black) and *Gfap*-TK (pink) GL261-bearing mice. (**B)** Box plot analysis of TCGA data of CD274 gene expression in GBM (*n*=163) and normal (Norm; *n*=207) patients. (**C)** Heat map overly of the scRNAseq gene expression intensity of *CD274* in GBM patients[4] (TAM and TAA clusters areas in **Supplementary Fig 3A)**. Expression levels are defined by color-coded expression (from yellow to red; Grey indicates that the transcript was not detected). (**D)** Kaplan-Meier curves assessing overall survival of GBM patients based on CD274 expression; n represent the number of patients per group. (**E**) Representative fluorescent images of primary mouse microglial cells (left) and primary astrocytes, stained for GFAP (green), IBA-1 (white), and nuclei (DAPI, magenta). scale bars, 20 μm (**F**) Mixed glial cultures were left untreated or subject to mild trypsinization[9]**,** isolating the microglial cells [MG (pure)]. Representative flow cytometry plots of CD11b/GLAST staining from each group are shown on the left and quantification analyses of $CD11b^+$ microglial cell frequencies are on the right (*n* = 4 biologically independent experiments). Data are shown as mean ± s.e.m. *P* values were determined by or two-sided Student's t-test (***, *P*<0.001). (**G**) Pure microglial cultures were prepared, treated with astrocytes conditioned medium (ACM) or control medium (Med), and co-cultured with GFP^+-GL261 cells for 48h (as in **Fig 4G**). Representative flow cytometry plots of GFP-gated GL261 cells from each group are shown on the left, and quantification analyses of cell death are on the right (*n* = 2 biologically independent experiments). Data are shown as mean ± s.e.m. *P*=0.678 by two-sided Student's t-test. (**H,I**) pure microglial cultures were prepared, treated, and co-incubated with isotype control or CSF1R blocking mAbs (25μg/ml) for 48h, as in (**Fig 4K**). Microglial cell death and proliferation were then analyzed by LDH assay (**H**) and CellTrace™ Violet staining (**I**). Representative flow cytometry plots are shown on the left and quantification analyses of the percentage of proliferating cells in each generation are on the right (*n* = 2). Data are representative of two independent experiments. Data are shown as mean ± s.e.m. *P* values were determined by two-sided Student's t-test; *P*= 0.89 (**H)**, or Two-way ANOVA, followed by Fisher's LSD post-hoc analysis; *P*>0.99 (**I**), ns, not significant. Box plot analysis of TCGA data of CSF1 (**J**) and CSF1R (**K**) gene expression in GBM (*n*=163) and normal (Norm; *n*=207) patients. (**L)** Heatmap overlay of CSF1/CSF1R ratio in the GBM TME, based on scRNAseq gene expression[4]. Ratio intensity is present by color; Blue – only CSF1 expressing cells, Yellow – the dual expression of CSF1 and CSF1R, and Red – cells that

only express CSF1R. (**M**,**N**) Kaplan-Meier curves assessing overall survival of GBM patient based on CSF1 and CSF1R expression; n represent the number of patients per group. Data are shown as mean ± s.e.m. *P* values were determined by or two-sided Student's t-test (expression data, **P*<0.01) or Log rank (Mantel-Cox) tests (survival, *P*<0.0001).

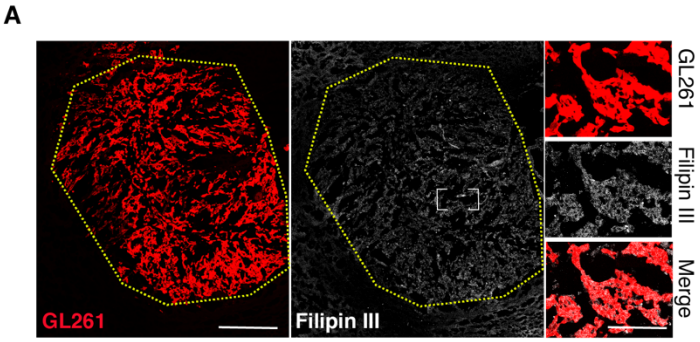
A
GL261
Filipin III
GL261
Filipin III
Merge

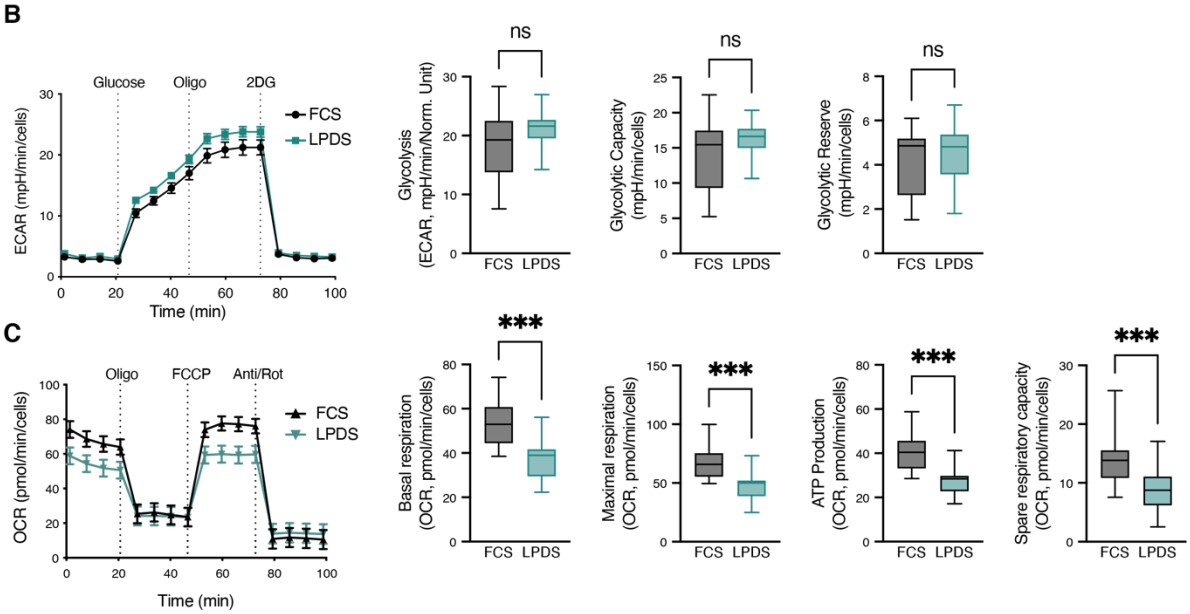
B
Glucose
Oligo
2DG
FCS
LPDS
ECAR (mpH/min/cells)
Time (min)
Glycolysis (ECAR, mpH/min/Norm. Unit)
Glycolytic Capacity (mpH/min/cells)
Glycolytic Reserve (mpH/min/cells)
ns
C
Oligo
FCCP
Anti/Rot
OCR (pmol/min/cells)
Basal respiration (OCR, pmol/min/cells)
Maximal respiration (OCR, pmol/min/cells)
ATP Production (OCR, pmol/min/cells)
Spare respiratory capacity (OCR, pmol/min/cells)
***

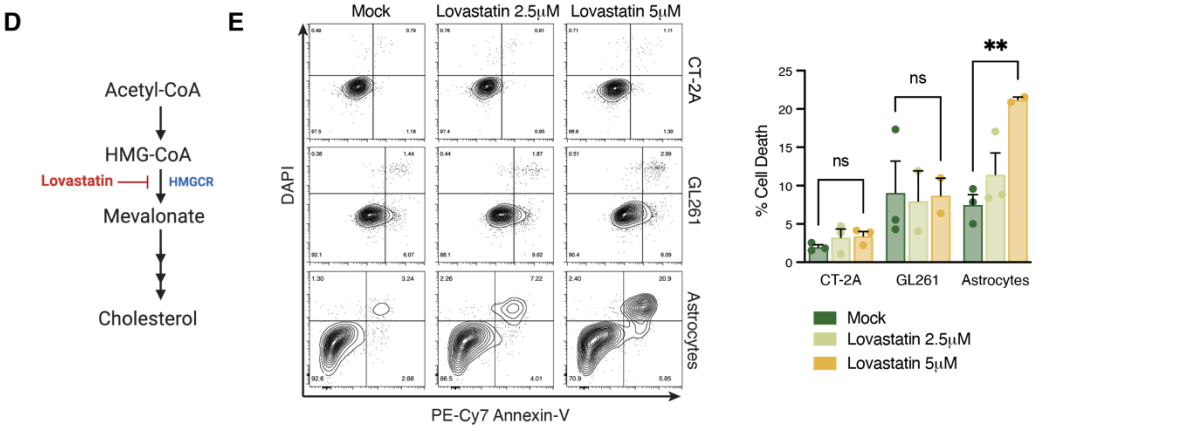
D
Acetyl-CoA
HMG-CoA
Lovastatin
HMGCR
Mevalonate
Cholesterol
E
Mock
Lovastatin 2.5μM
Lovastatin 5μM
CT-2A
GL261
Astrocytes
DAPI
PE-Cy7 Annexin-V
% Cell Death
ns
**
Mock
Lovastatin 2.5μM
Lovastatin 5μM

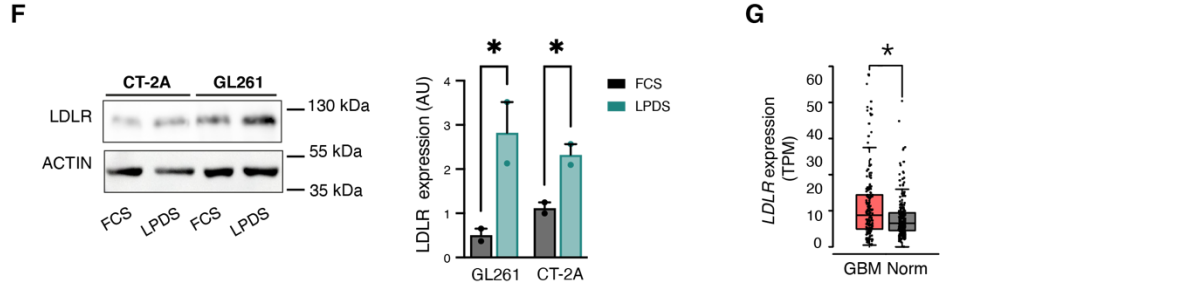
F
CT-2A
GL261
LDLR
ACTIN
130 kDa
55 kDa
35 kDa
FCS
LPDS
LDLR expression (AU)
G
LDLR expression (TPM)
GBM Norm
*

Supplementary Figure 6. Astrocyte-derived cholesterol support glioma survival. (A) Representative immunofluorescence images of cholesterol accumulation (Filipin III, white) in the GBM tumor (tdTomato+ GL261 cells, red), Tumor margins are indicated in yellow (n = 3 biologically independent samples). Scale bars, 400 μm (right), 150 μm (left). (**B,C)** Real-time changes in the ECAR (**B**) and OCR (**C**) of CT-2A glioma cells, cultured in media supplemented with full serum (FCS) or lipoprotein-deprived serum (LPDS) for 18 h and measured using Seahorse. Oligo, oligomycin; FCCP, carbonyl cyanide4-(trifluoromethoxy) phenylhydrazone; R/A, rotenone plus antimycin A; 2-DG, 2-deoxy-d-glucose. Glycolysis, glycolytic capacity and glycolytic reserve are extracted from ECAR reading, and basal respiration, ATP production, Maximal respiration, and spare respiratory capacity were determined based on OCR. Data are representative of two independent experiments (n = 6 technical replicates per experiment). (**D**) Scheme of cholesterol synthesis inhibition by HMGCR-inhibitor lovastatin. (**E**) Representative flow cytometry plots and quantification analyses of Annexin V/DAPI staining comparing astrocytes with CT-2A and GL261 cells after a 3-day treatment with the lovastatin. (n = 3 biologically independent experiments). (**F**) Representative immunoblot and quantification analyses comparing LDLR protein levels in with CT-2A and GL261 cells cluttered for 2 days in FCS or LPDS supplemented media. (n = 3 biologically independent experiments). (**G**) Box plot analysis of TCGA gene expression for *LDLR* in normal (n=207) or GBM patients (n=163). n represents the number of patients per group. Data are shown as mean ± s.e.m. P values were determined by two-sided Student's t-tests (**B,C,F** and **G**) or by one-way ANOVA, followed by Fisher's LSD post-hoc analysis (**E**). *P<0.05, **P<0.01, ***P<0.001.

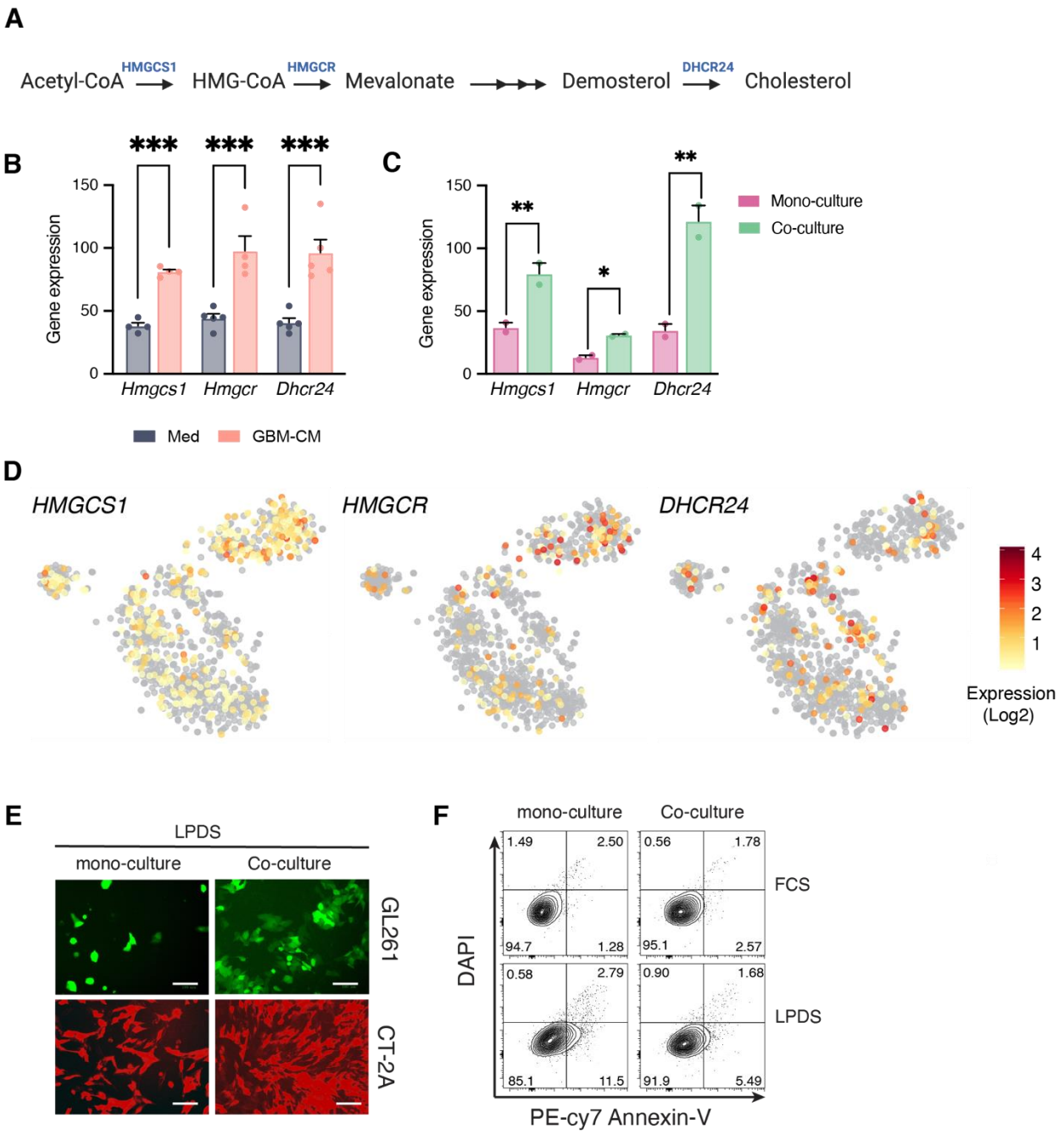

Supplementary Figure 7. Astrocyte-derived cholesterol support glioma survival. (A) Scheme of *de-novo* cholesterol synthesis pathway. (**B,C)** qPCR analyses of *Hmgcs1*, *Hmgcr*, and *Dhcr24* expression in astrocytes treated with GBM-CM (**B**) or co-incubated for 24h with GL261 (**C**); expression normalized to *Ppia* (*n* = 4 biologically independent experiments). (**D)** Heat map overly of the scRNAseq gene expression intensity of *HMGCS1, HMGCR, and DHC24* in tumor-associated astrocytes from GBM patients[4] (astrocyte cluster as in **Supplementary Fig 3A)**. Expression levels are defined by color-coded expression (from yellow to red; Grey indicates that

the transcript was not detected). (**E**,**F)** Analysis of LPDS-induced glioma cell death, in the presence or absence of primary astrocytes, by Annexin-V assay. (**E**) Representative fluorescent images of murine GFP^+-GL261 and $tdTomato^+$-CT-2A glioma cells were co-cultured with or without primary mouse astrocytes (n = 4 biologically independent experiments). (**F**) Representative flow cytometry plots and quantification analyses of Annexin V/DAPI staining comparing human U87EGFRvIII[10] glioma cells co-cultured with or human primary astrocytes for 5 days (n = 3 biologically independent experiments). Data are shown as mean ± s.e.m. P values were determined by a two-sided Student's t-test (**B** and **C**). *P<0.05, **P<0.01, ***P<0.001.

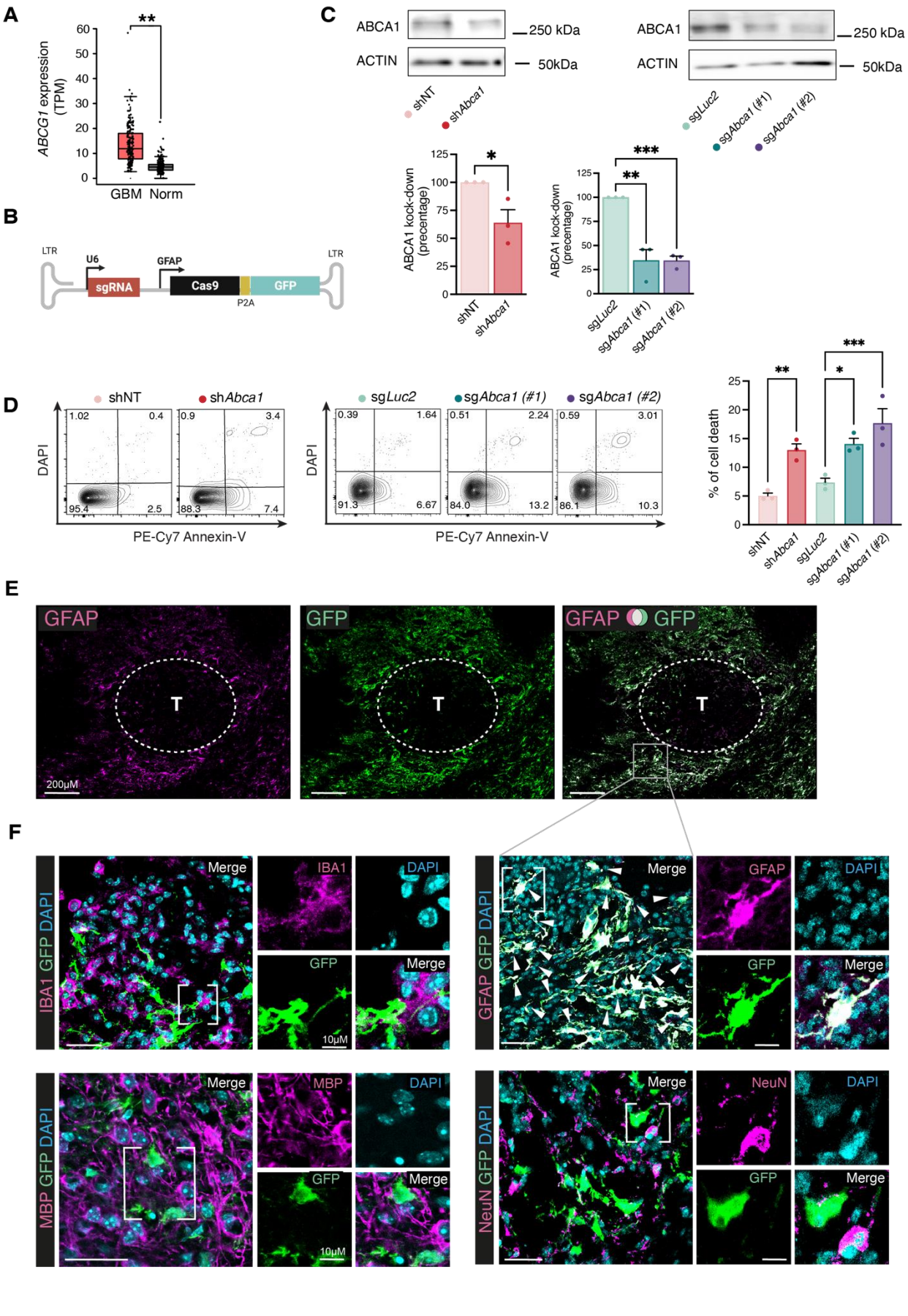
A
ABCG1 expression (TPM)
GBM
Norm
B
LTR
U6
sgRNA
GFAP
Cas9
P2A
GFP
LTR
C
ABCA1
ACTIN
250 kDa
50kDa
shNT
shAbca1
sgLuc2
sgAbca1 (#1)
sgAbca1 (#2)
ABCA1 kock-down (precentage)
D
shNT
shAbca1
sgLuc2
sgAbca1 (#1)
sgAbca1 (#2)
DAPI
PE-Cy7 Annexin-V
% of cell death
E
GFAP
GFP
T
200μM
F
IBA1 GFP DAPI
MBP GFP DAPI
GFAP GFP DAPI
NeuN GFP DAPI
Merge
10μM

Supplementary Figure 8. Astrocytic expression of *ABCG1*, *ABCA1*, and astrocyte-specific lentiviruses. (A) Box plot analysis of TCGA gene expression for *ABCG1* in normal (Norm; *n*=207) or GBM (*n*=163) patients. n represents the number of patients per group **(B-D)** Primary astrocytes were transduced with RNAi encoding lentiviruses [Non-targeting shRNA (shNT) or A*bca1*-targeting shRNA (sh*Abca1*); Schematic map of the astrocyte-specific shRNA lentiviral vector in **Fig. 6F**], Or astrocyte-specific CRISPR-Cas9 lentivirus targeting the luciferase gene (sg*Luc2*; control), or *Abca1* sg*Abca1* (#1) and sg*Abca1* (#2); Schematic map of the astrocyte-specific CRISPR-Cas9-sgRNA lentiviral vector in (**B**). shRNA and sgRNA sequences are detailed in **Supplementary Table 1**. Transduced astrocytes were then co-cultured with CT-2A glioma cells in LPDS-media for 5 days, and LPDS-induced glioma cell death was determined by Annexin-V assay. **(C)** Representative immunoblot and quantification analyses comparing ABCA1 protein levels in transduced astrocytes (*n* = 3 biologically independent experiments). **(D)** Representative flow cytometry plots of CT-2A glioma cells co-cultured for 5 days with transduced astrocytes are shown on the left and quantification analyses on the right (*n* = 3 biologically independent experiments). Data are shown as mean ± s.e.m. *P* values were determined by a two-sided Student's t-test (**C**) or by one-way ANOVA (**C**, **D**). **P*<0.05, ***P*<0.01, ****P*<0.001. (**E,F**) Expression of astrocyte-specific GFP-expressing *Gfap*-shRNA lentiviruses-injected GBM-bearing mice. **(E)** Representative immunofluorescence images of GFP (green) and GFAP (astrocytes, magenta), scale bars, 400 μm **(F)** Representative immunofluorescence images of GFP expression (green) and cell makers for TAMs (IBA1, magenta), oligodendrocytes (MBP, magenta), astrocytes (GFAP, magenta), or neurons (NeuN, magenta). Colocalization (white) is identified by white arrowheads. Large scale image on the left, insert (white box) on the right. scale bars, 40 μm, scale bar for insert 10 μM. Data are representative of two independent experiments with *n* = 3 mice/group.

Supplementary Table 1. Sequences used for generating ABCA1 RNAi vectors

ID	Name	Sequence (5'->3')
1	shNT[11]	GAGTGCCACTTTCCGAATAAA
2	sh*Abca1*	GCGCGATAGCGCTAATAATTT
3	gfaABC1D	GATCTAACATATCCTGGTGTGGAGTAGGGGACGCTGCTCTGACAGAGGCTCGGGGGCCTGA GCTGGCTCTGTGAGCTGGGGAGGAGGCAGACAGCCAGGCCTTGTCTGCAAGCAGACCTGGC AGCATTGGGCTGGCCGCCCCCCAGGGCCTCCTCTTCATGCCCAGTGAATGACTCACCTTGGC ACAGACACAATGTTCGGGGTGGGCACAGTGCCTGCTTCCCGCCGCACCCCAGCCCCCCTCA AATGCCTTCCGAGAAGCCCATTGAGCAGGGGGCTTGCATTGCACCCCAGCCTGACAGCCTG GCATCTTGGGATAAAAGCAGCACAGCCCCCTAGGGGCTGCCCTTGCTGTGTGGCGCCACCG GCGGTGGAGAACAAGGCTCTATTCAGCCTGTGCCCAGGAAAGGGGATCAGGGGATGCCCAG GCATGGACAGTGGGTGGCAGGGGGGGAGAGGAGGGCTGTCTGCTTCCCAGAAGTCCAAGGA CACAAATGGGTGAGGGGAGAGCTCTCCCCATAGCTGGGCTGCGGCCCAACCCCACCCCCTC AGGCTATGCCAGGGGGTGTTGCCAGGGGCACCCGGGCATCGCCAGTCTAGCCCACTCCTTC ATAAAGCCCTCGCATCCCAGGAGCGAGCAGAGCCAGAGCAGGTTGGAGAGGAGACGCATCA CCTCCGCTGCTCGCA
4	sg*Luc2*[12]	CACCGTTGGCGCTCAACTTTTACGA
5	Sg*Abca1* (#1)	CACCGGAGAGTCACTCACCCGGACA
6	sg*Abca1* (#2)	CACCGTTGGCGCTCAACTTTTACGA
7	sgRNA sequencing primer	TACGTGACGTAGAAAGTA

Supplementary Table 2. Functional enrichment analysis of tumor-associated astrocytes

ID	Term ID	Term Name	P_{adj}
1	GO:0007049	Cell cycle	2.810×10^{-17}
2	GO:0008152	Metabolic process	7.455×10^{-18}
3	GO:0022402	Cell cycle process	3.882×10^{-19}
4	GO:0034097	Response to cytokine	5.456×10^{-19}
5	GO:0044237	Cellular metabolic process	7.852×10^{-19}
6	GO:0065009	Regulation of molecular function	1.892×10^{-17}
7	GO:0071345	Cellular response to cytokine stimulus	6.642×10^{-18}
8	GO:0071840	Cellular component organization or biogenesis	1.606×10^{-26}
9	GO:1903047	Mitotic cell cycle process	7.675×10^{-17}
10	GO:0000278	Mitotic cell cycle	1.572×10^{-14}
11	GO:0006950	Response to stress	1.257×10^{-15}
12	GO:0010646	Regulation of cell communication	5.250×10^{-16}
13	GO:0071704	Organic substance metabolic process	9.935×10^{-15}
14	GO:0002376	Immune system process	1.398×10^{-11}
15	GO:0006807	Nitrogen compound metabolic process	1.895×10^{-13}
16	GO:0006725	Cellular aromatic compound metabolic process	1.421×10^{-12}
17	GO:0006139	Nucleobase-containing compound metabolic process	2.368×10^{-12}
18	GO:0009893	Positive regulation of metabolic process	9.465×10^{-14}
19	GO:0010604	Positive regulation of macromolecule metabolic process	4.478×10^{-12}
20	GO:0031325	Positive regulation of cellular metabolic process	1.258×10^{-11}
21	GO:0034641	Cellular nitrogen compound metabolic process	1.218×10^{-11}
22	GO:0044238	Primary metabolic process	4.418×10^{-12}
23	GO:0046483	Heterocycle metabolic process	4.138×10^{-13}
24	GO:0051173	Positive regulation of nitrogen compound metabolic process	9.325×10^{-12}
25	GO:0001816	Cytokine production	2.656×10^{-10}
26	GO:0002682	Regulation of immune system process	6.102×10^{-11}
27	GO:0006952	Defense response	1.819×10^{-8}
28	GO:0006260	DNA replication	9.952×10^{-9}
29	GO:0001819	Positive regulation of cytokine production	7.640×10^{-8}
30	GO:0006261	DNA-dependent DNA replication	7.931×10^{-7}
31	GO:0008283	Cell population proliferation	6.102×10^{-8}
32	GO:0010547	Positive regulation of cell communication	4.337×10^{-9}
33	GO:0031347	Regulation of defense response	2.701×10^{-10}
34	GO:0031349	Positive regulation of defense response	2.801×10^{-8}
35	GO:0035458	Cellular response to interferon-beta	1.396×10^{-7}
36	GO:0044260	Cellular macromolecule metabolic process	4.949×10^{-8}
37	GO:0044770	Cell cycle phase transition	2.302×10^{-9}
38	GO:0044085	Cellular component biogenesis	2.027×10^{-10}
39	GO:0043170	Macromolecule metabolic process	2.001×10^{-10}
40	GO:0051301	Cell division	1.971×10^{-9}
41	GO:0051726	Regulation of cell cycle	2.324×10^{-8}
42	GO:0090304	Nucleic acid metabolic process	1.122×10^{-10}
43	GO:1901987	Regulation of cell cycle phase transition	7.436×10^{-8}
44	GO:1901990	Regulation of mitotic cell cycle phase transition	1.709×10^{-7}
45	GO:0045935	Positive regulation of nucleobase-containing compound metabolic process	2.624×10^{-7}
46	GO:0042127	Regulation of cell population proliferation	4.890×10^{-7}
47	GO:0034645	Cellular macromolecule biosynthetic process	3.575×10^{-6}
48	GO:0033993	Response to lipid	7.113×10^{-6}
49	GO:0031323	Regulation of cellular metabolic process	6.053×10^{-6}
50	GO:0019222	Regulation of metabolic process	1.206×10^{-6}
51	GO:0008284	Positive regulation of cell population proliferation	2.054×10^{-5}
52	GO:0002263	Cell activated involved in immune response	5.501×10^{-5}
53	GO:0000280	Nuclear division	1.370×10^{-6}
54	GO:0000082	G1/S transition of mitotic cell cycle	1.451×10^{-4}
55	GO:0002697	Regulation of immune effector process	1.190×10^{-4}
56	GO:0006955	Immune response	9.476×10^{-4}
57	GO:0008608	Attachment of spindle microtubules to kinetochore	3.878×10^{-3}
58	GO:0019221	Cytokine-mediated signaling pathway	2.007×10^{-4}
59	GO:0030335	Positive regulation of cell migration	9.829×10^{-5}
60	GO:0032270	Positive regulation of cellular protein metabolic process	7.465×10^{-5}
61	GO:0050776	Regulation of immune response	1.550×10^{-5}
62	GO:0060255	Regulation of macromolecule metabolic process	1.416×10^{-6}
63	GO:0060759	Regulation of response to cytokine stimulus	6.124×10^{-5}
64	GO:0080090	Regulation of primary metabolic process	2.290×10^{-5}
65	GO:1902806	Regulation of cell cycle G1/S phase transition	3.190×10^{-3}
66	GO:0140014	Mitotic nuclear division	1.703×10^{-5}

67	GO:0060760	Positive regulation of response to cytokine stimulus	1.187×10^{-3}
68	GO:0051247	Positive regulation of protein metabolic process	3.679×10^{-4}
69	GO:0010556	Regulation of macromolecule biosynthetic process	3.854×10^{-4}
70	GO:0006091	Generation of precursor metabolites and energy	5.548×10^{-4}

Supplementary Table 2. Functional enrichment analysis of differently regulated transcripts from tumor-associated astrocytes based on Gene Ontology (GO).

Supplementary Table 3. Functional enrichment analysis of human tumor-associated astrocytes

ID	Term ID	Term Name	ES	FDR
1	R-HSA-3656243	Defective ST3GAL3 causes MCT12 and EIEE15	0.98662	0.03965
2	R-HSA-191273	Cholesterol biosynthesis	0.64482	0.03965
3	R-HSA-389661	Glyoxylate metabolism and glycine degradation	0.63704	0.03965
4	R-HSA-6799198	Complex I biogenesis	0.55068	0.03965
5	R-HSA-163200	Respiratory electron transport, ATP synthesis by chemiosmotic coupling, and heat production by uncoupling proteins.	0.5376	0.03965
6	R-HSA-611105	Respiratory electron transport	0.5357	0.03965
7	R-HSA-1655829	Regulation of cholesterol biosynthesis by SREBP (SREBF)	0.52005	0.03965
8	R-HSA-2426168	Activation of gene expression by SREBF (SREBP)	0.51517	0.03965
9	R-HSA-1428517	The citric acid (TCA) cycle and respiratory electron transport	0.43726	0.03965
10	R-HSA-168249	Innate Immune System	-0.30387	0.03965
11	R-HSA-9006934	Signaling by Receptor Tyrosine Kinases	-0.33193	0.03965
12	R-HSA-372790	Signaling by GPCR	-0.33459	0.03965
13	R-HSA-196854	Metabolism of vitamins and cofactors	-0.38108	0.03965
14	R-HSA-425407	SLC-mediated transmembrane transport	-0.39824	0.03965
15	R-HSA-1280215	Cytokine Signaling in Immune system	-0.39854	0.03965
16	R-HSA-913531	Interferon Signaling	-0.42312	0.03965
17	R-HSA-373760	L1CAM interactions	-0.42924	0.03965
18	R-HSA-449147	Signaling by Interleukins	-0.44046	0.03965
19	R-HSA-500792	GPCR ligand binding	-0.45853	0.03965
20	R-HSA-373755	Semaphorin interactions	-0.46668	0.03965
21	R-HSA-6806834	Signaling by MET	-0.51052	0.03965
22	R-HSA-76005	Response to elevated platelet cytosolic Ca2+	-0.53623	0.03965
23	R-HSA-909733	Interferon alpha/beta signaling	-0.53748	0.03965
24	R-HSA-3000178	ECM proteoglycans	-0.58288	0.03965
25	R-HSA-3000171	Non-integrin membrane-ECM interactions	-0.60099	0.03965
26	R-HSA-202733	Cell surface interactions at the vascular wall	-0.60219	0.03965
27	R-HSA-373076	Class A/1 (Rhodopsin-like receptors)	-0.61315	0.03965
28	R-HSA-1566948	Elastic fibre formation	-0.62358	0.03965
29	R-HSA-1474244	Extracellular matrix organization	-0.62407	0.03965
30	R-HSA-375276	Peptide ligand-binding receptors	-0.63294	0.03965
31	R-HSA-6785807	Interleukin-4 and Interleukin-13 signaling	-0.63426	0.03965
32	R-HSA-400685	Sema4D in semaphorin signaling	-0.63503	0.03965
33	R-HSA-381426	Regulation of Insulin-like Growth Factor (IGF) transport and uptake by Insulin-like Growth Factor Binding Proteins (IGFBPs)	-0.64225	0.03965
34	R-HSA-9645723	Diseases of programmed cell death	-0.65146	0.03965
35	R-HSA-8875878	MET promotes cell motility	-0.65289	0.03965
36	R-HSA-1442490	Collagen degradation	-0.65325	0.03965
37	R-HSA-6783589	Interleukin-6 family signaling	-0.65494	0.03965
38	R-HSA-877300	Interferon gamma signaling	-0.66473	0.03965
39	R-HSA-76009	Platelet Aggregation (Plug Formation)	-0.6806	0.03965
40	R-HSA-1474228	Degradation of the extracellular matrix	-0.68368	0.03965
41	R-HSA-449836	Other interleukin signaling	-0.68368	0.03965
42	R-HSA-210991	Basigin interactions	-0.68665	0.03965
43	R-HSA-3000170	Syndecan interactions	-0.69992	0.03965
44	R-HSA-3000157	Laminin interactions	-0.71571	0.03965
45	R-HSA-8874081	MET activates PTK2 signaling	-0.7177	0.03965
46	R-HSA-1650814	Collagen biosynthesis and modifying enzymes	-0.71836	0.03965
47	R-HSA-8948216	Collagen chain trimerization	-0.73086	0.03965
48	R-HSA-198933	Immunoregulatory interactions between a Lymphoid and a non-Lymphoid cell	-0.73656	0.03965
49	R-HSA-1474290	Collagen formation	-0.73969	0.03965
50	R-HSA-5357786	TNFR1-induced proapoptotic signaling	-0.74918	0.03965
51	R-HSA-446353	Cell-extracellular matrix interactions	-0.77086	0.03965
52	R-HSA-216083	Integrin cell surface interactions	-0.77262	0.03965
53	R-HSA-196807	Nicotinate metabolism	-0.77888	0.03965
54	R-HSA-2022090	Assembly of collagen fibrils and other multimeric structures	-0.79098	0.03965
55	R-HSA-197264	Nicotinamide salvaging	-0.8154	0.03965
56	R-HSA-6783783	Interleukin-10 signaling	-0.885	0.03965
57	R-HSA-380108	Chemokine receptors bind chemokines	-0.91066	0.03965
58	R-HSA-2243919	Crosslinking of collagen fibrils	-0.93	0.03965
59	R-HSA-173736	Alternative complement activation	-0.9999	0.03965
60	R-HSA-6799990	Metal sequestration by antimicrobial proteins	-1	0.03965

Supplementary Table 3. Functional enrichment analysis of differently regulated transcripts from human tumor-associated astrocytes[4] based on the Reactome database. ES - enrichment score comparing the two clusters, FDR - false discovery rate. FDR<0.05.

Supplementary References

1. Buch T, Heppner FL, Tertilt C, *et al*. A Cre-inducible diphtheria toxin receptor mediates cell lineage ablation after toxin administration. *Nat Methods*. Jun 2005;2(6):419-26. doi:10.1038/nmeth762

2. Schreiner B, Romanelli E, Liberski P, *et al*. Astrocyte Depletion Impairs Redox Homeostasis and Triggers Neuronal Loss in the Adult CNS. *Cell Rep*. Sep 1 2015;12(9):1377-84. doi:10.1016/j.celrep.2015.07.051

3. Takenaka MC, Gabriely G, Rothhammer V, *et al*. Control of tumor-associated macrophages and T cells in glioblastoma via AHR and CD39. *Nat Neurosci*. May 2019;22(5):729-740. doi:10.1038/s41593-019-0370-y

4. Darmanis S, Sloan SA, Croote D, *et al*. Single-Cell RNA-Seq Analysis of Infiltrating Neoplastic Cells at the Migrating Front of Human Glioblastoma. *Cell Rep*. Oct 31 2017;21(5):1399-1410. doi:10.1016/j.celrep.2017.10.030

5. Wu YE, Pan L, Zuo Y, Li X, Hong W. Detecting Activated Cell Populations Using Single-Cell RNA-Seq. *Neuron*. Oct 11 2017;96(2):313-329 e6. doi:10.1016/j.neuron.2017.09.026

6. Zhong S, Zhang S, Fan X, *et al*. A single-cell RNA-seq survey of the developmental landscape of the human prefrontal cortex. *Nature*. Mar 22 2018;555(7697):524-528. doi:10.1038/nature25980

7. Collardeau-Frachon S, Scoazec JY. Vascular development and differentiation during human liver organogenesis. *Anat Rec (Hoboken)*. Jun 2008;291(6):614-27. doi:10.1002/ar.20679

8. Kambach DM, Halim AS, Cauer AG, *et al*. Disabled cell density sensing leads to dysregulated cholesterol synthesis in glioblastoma. *Oncotarget*. Feb 28 2017;8(9):14860-14875. doi:10.18632/oncotarget.14740

9. Lin L, Desai R, Wang X, Lo EH, Xing C. Characteristics of primary rat microglia isolated from mixed cultures using two different methods. *J Neuroinflammation*. May 8 2017;14(1):101. doi:10.1186/s12974-017-0877-7

10. Villa GR, Hulce JJ, Zanca C, *et al*. An LXR-Cholesterol Axis Creates a Metabolic Co-Dependency for Brain Cancers. *Cancer Cell*. Nov 14 2016;30(5):683-693. doi:10.1016/j.ccell.2016.09.008

11. Mayo L, Trauger SA, Blain M, *et al*. Regulation of astrocyte activation by glycolipids drives chronic CNS inflammation. *Nat Med*. Oct 2014;20(10):1147-56. doi:10.1038/nm.3681

12. Hart T, Chandrashekhar M, Aregger M, *et al*. High-Resolution CRISPR Screens Reveal Fitness Genes and Genotype-Specific Cancer Liabilities. *Cell*. Dec 3 2015;163(6):1515-26. doi:10.1016/j.cell.2015.11.015